

## **Conventional and non-conventional differencing in time-lapse**

Vanja Vracar and Dr. Robert J. Ferguson

### **ABSTRACT**

We present a comparison between the conventional time-lapse differencing and the new non-conventional differencing method based on the inverse data matrix. We use 2D variable velocity models and their corresponding migrated synthetic seismograms to represent three snapshots in time-lapse. Conventional differencing performed on the time-lapse data captures no amplitude patterns and proves to be of limited use in reservoir characterization. On the other hand, non-conventional differencing by inverse data matrix captures some amplitude patterns and offers more intuitive plots for interpretation.

### **INTRODUCTION**

Seismic imaging is a process through which waves recorded on the surface are mapped into an image of the subsurface (Ferguson, 2009a), is heavily applied in industry. In particular, seismic imaging is used in hydrocarbon reservoir exploration and development (Huang et al., 1998). Success there is directly related to familiarity with reservoirs (Lines and Newrick, 2008). Imaging is not a difficult task; when dealing with reservoirs with long production history, however, it becomes a challenging task when dealing with reservoirs with short to no production history (Vracar, 2007). To study reservoirs and its properties actual or synthetic testing and modelling take place (Cosse, 1993). This process generates subsurface images used for reservoir monitoring or evaluation (Ferguson, 2009a).

As production influences reservoir properties with fluid flow displacement, reservoirs are observed in time-lapse (Cheng et al., 2009). Time-lapse observation images are generated in various production days (Zou et al., 2004). The spatio-temporal changes in hydrocarbon reserves are evaluated to define their effects on reservoir properties and further exploitation planning (Jin and Chen, 2008). Numerous analysis procedures exist to optimize production. Some of these analysis include: core, pressure transient, fracture, stratigraphic dip, conventional differencing, etc (Vracar, 2007). Of these analysis procedures, conventional seismic differencing is of interest here.

Many studies focus on seismic differencing methods and analyses. Huang et al. (1998) observe amplitude patterns on seismic difference models in time-lapse. They generate three synthetic models for comparison. Three models focus on evaluation of: production history only, measured differences in physical parameters only and combination of the previous two. The study points the importance of monitoring/modelling differences in a producing reservoir for further reservoir characterization. Schinelli (2006) highlights complex seismic attributes, such as signal to noise ratio and tuning, to be valuable when appraising conventional amplitude differencing. He proposes complex attributes to significantly limit fluid flow displacement observation on simple amplitude subtraction imaging. Bertrand et al. (2005) present a method to highlight amplitude differencing through the removal of traveltimes between base and monitor models. Jin and Chen (2008) propose methods to enhance time-lapse seismic anomaly and reduce noise decomposing on differenced models

using wavelet transform and filters.

Berkhout and Verschuur (2005) develop what we will call non-conventional seismic differencing. Their method is based on linear algebra where they situate data into a matrix and then generate inverse data space through matrix inversion. Berkhout and Verschuur (2005) illustrate this space as suitable for data processing in time-lapse, especially to surface related multiple elimination (SRME).

In this project, we evaluate time-lapse conventional and non-conventional seismic differencing through numerical experiments of 2D data sets. Namely, we evaluate some aspects of Berkhout and Verschuur (2005) data processing method for use in reservoir characterization. We evaluate how the inverse data space directly mapped into estimates of time-lapse differences (Inannen, 2009) benefit reservoir studies. We implement MATLAB code to illustrate both 2D data imaging after conventional and non-conventional seismic differencing. We analyze fluid flow displacement imaging, its amplitude and phase imaging in time-lapse. We compare results after conventional and non-conventional seismic differencing and examine its use in reservoir characterization. Finally, we evaluate algorithms' computation time and look for future improvements and research opportunities.

The designed time-lapse study will follow two workflows. Table 1 captures workflow applied to 2D velocity plots. There are four stages: I) forward seismic modelling, II) migration III) conventional and IV) non-conventional differencing.

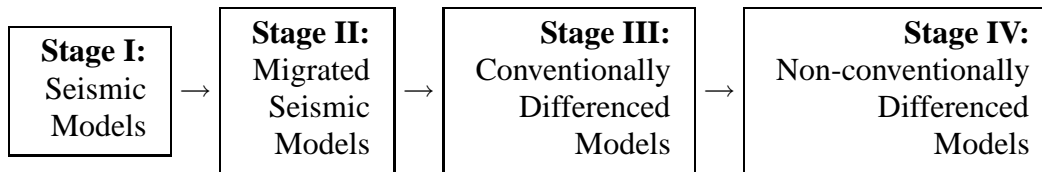


Table 1. 2D modelling workflow consists of four stages. They are applied and evaluated in order shown.

In Stage I synthetic seismic modelling, employing finite difference algorithm as exploding reflector models. In Stage II velocity models and synthetics are depth migrated employing Split-step Fourier (SSF) migration (Stoffa et al., 1990). In Stage III migrated sections are differenced conventionally and evaluated. In Stage IV migrated sections are differenced non-conventionally employing some aspects of Berkhout and Verschuur (2005) method, and also evaluated.

Both conventional and nonconventional differencing method show valuable. We expect to find conventional differencing fast. It will trace large scale reservoir characteristics with fluid flow displacement and no certain amplitude patterns. Non-conventional differencing, although requiring longer computation time, will trace large and fine scale reservoir characteristics with fluid flow displacement. Also, non-conventional differencing is expected to capture some amplitude patterns.

## THEORY

We use the 10<sup>th</sup> Comparative Solution Project data set (Christie and Blunt, 2001). Data set models, monitoring one producing and two injecting wells, a 100 % oil saturated reservoir as water saturation develops and breaks through in production after 28 days (Aarnes et al., 2007). A public domain simulator, consisting of numerous MATLAB routines designed by SINTEF ICT, models saturation advancement (Aarnes et al., 2007). Assume both oil and water, to be incompressible, irreducible and immiscible, namely they are fully displaced by one another, with no blending or density changes (Christie and Blunt, 2001). The workflow is to take velocity models, to zero-offset seismic models, migrate them and allow differencing, that is conventionally and non-conventionally.

### Velocity and seismic synthetics modelling

A laterally varying 2D velocity model is assumed to model the above reservoir in time-lapse. Suppose waterfronts to dip at 90°. Velocity model invokes finite difference method and generates synthetic data. Synthetics image 2D zero-offset exploding reflector gather.

### Migration modelling

Stoffa et al. (1990) introduce the SSF migration algorithm, which handles lateral changes in velocity at each depth level. Also, the algorithm takes into account dipping events. Assume 2D propagation of compressional (P) waves in acoustic medium and constant density. Wave propagation is defined as (Stoffa et al., 1990) :

$$\nabla^2 d - u^2 \frac{\partial^2}{\partial t^2} d = 0, \quad (1)$$

where  $t$ ,  $d = d(x, z, t)$  and  $u = u(x, z)$  are time, pressure and slowness, respectively. The inverse of the half of the propagation velocity  $u(x, z) = 2/v(x, z)$ , where  $v$ ,  $x$ ,  $z$  are velocity, horizontal and vertical distance, respectively, denotes slowness. The above statement is imperative by the exploding reflector model when zero-offset data is migrated (Mi, 2002). As the migration by SSF takes place partially in the frequency domain, equation (1) is Fourier transformed to:

$$\nabla^2 D + \omega^2 u^2 + D = 0, \quad (2)$$

where  $\omega$  is frequency and  $D = D(x, z, \omega) = \int_{-\infty}^{+\infty} d(x, z, t) e^{-i\omega t} dt$ . Now, Stoffa et al. (1990) decompose the slowness term from equation (2) in two components:

$$u(x, z) = u_0(z) + \Delta u(x, z), \quad (3)$$

where  $u_0(z)$  and  $\Delta u(x, z)$  are the reference and perturbation slowness. The reference slowness in equation (3) is the mean of  $u(x, z)$  and as per Ferguson and Margrave (1999) named stationary. The perturbation slowness accommodates all velocity variations, hence is nonstationary (Ferguson and Margrave, 1999). Thus the homogeneous wave equation transforms into the inhomogeneous, constant-slowness wave equation (Stoffa et al., 1990):

$$\nabla^2 D + \omega^2 u_0^2 D = -U(x, z, \omega), \quad (4)$$

where  $U(x, z, \omega) = \omega^2[2u_0\Delta u(x, z, \omega) + \Delta u^2(x, z, \omega)]D$  is a source like-term. The second order term in equation (4) is ignored as perturbation slowness is small when compared to the reference slowness.

The solution of equation (4) is summarized in three steps (Du, 2007):

I. Transform wavefield from the spatial to the wavenumber domain and apply a phase-shift based on the vertical wavenumber,  $k_z$ , computed by the reference slowness:

$$D^*(z + \Delta z, k_x, \omega) = D(z, k_x, \omega)e^{\pm i\sqrt{\omega^2 u_0^2 - k_x^2} \Delta z}, \quad (5)$$

where  $k_x$  denotes horizontal wavenumber.

II. Inverse Fourier equation (5), that is transform  $D^*(z + \Delta z, k_x, \omega)$  back to  $D^*(z + \Delta z, x, \omega)$  as:

$$D^*(z + \Delta z, x, \omega) = \int_{-\infty}^{+\infty} D(z + \Delta z, k_x, \omega)e^{-ik_x x} dk_x. \quad (6)$$

III. In the space and frequency domains, generated by equation (6), apply a second phase-shift due to the perturbation in the slowness:

$$D(z + \Delta z, x, \omega) = D^*(z + \Delta z, x, \omega)e^{\pm i\left(\frac{\omega}{v(x,z)} - \frac{\omega}{v_0(z)}\right)\Delta z}. \quad (7)$$

Now, integrate equation (7) over all frequencies of interest to deliver the migrated data (Mi, 2002).

### Difference modelling

Time-lapse migrated seismic models are presented as matrices  $D_i$ , where  $i$  denotes time step. These sections are differenced employing conventional matrix subtraction:

$$D_{diff} = D_i - D_{i+1}. \quad (8)$$

Equation (8) captures large scale physical changes of reservoir as production progresses. Namely, hydrocarbon volume and its displacement changes are expected to be interpretable for use in enhanced recovery schemes development and monitoring.

### Improved difference modelling

The Berkhout and Verschuur (2005) method is developed as an improvement to conventional differencing focusing primarily on SRME concept. We give a brief review of the SRME method presented in Berkhout and Verschuur (2005) and tie it to differencing. The method places initial migrated data in matrix  $D_i$  to represent base study. Subtracted migrated time step data are placed in matrices denoted as  $D_{i+1}$ 's. All matrices have complex scaled entries in temporal frequency domain and their rows and columns denote receiver and shot recordings, respectively. Further, Berkhout and Verschuur (2005) define the data matrices as:

$$D_i(z_0, z_0) = P(z_0, z_0)X_0(z_0, z_0)S(z_0), \quad (9)$$

where  $P$ ,  $X_0$  and  $S$  denote receiver array at the surface  $z_0$ , transfer function and source array at the surface respectively. The transfer function in equation (9) relates input and output data due to subsurface conditions. A feedback model is developed for recording a very complicated data set with numerous surface-related multiples (Berkhout and Verschuur, 2005):

$$D = D_0 + (D_0A)D_0 + (D_0A)^2D_0 + \dots, \quad (10)$$

where  $A = S^{-1}R^*P^{-1}$  and  $R^*$  is surface reflectivity and  $D_0$  contains primaries only. The surface operator  $A$  does not contain traveltime. The series expansion in equation (10) can be expressed as continuous form through the use of Binomial expansion:

$$D = [I - D_0A]^{-1}D_0. \quad (11)$$

Multiplication with  $(D_0A)$  in equation (10) and (11) represents spatial convolution, that is adding one roundtrip through subsurface (Berkhout and Verschuur, 2005). Simplifying equation (11), we get:

$$D = D_0 + D_0AD, \quad (12)$$

that is a multiple scattering equation of known Lippmann-Schwinger structure (Inannen, 2010). Equation (12) represents the theoretical bases of multiple removal algorithms such as SRME (Berkhout, 2006). Equation (12) is the surface-related version of equation (11). Employing matrix inversion, we move from multiple scattering data in forward data space (FDS), described by equation (11), to inverse data space (IDS) (Berkhout, 2006):

$$D^{-1} = D_0^{-1} - A. \quad (13)$$

Equation (13) describes a much simpler data set based on surface-free earth response and surface related properties at and around zero time.

To analyze data in time-lapse, define migrated base study as (Berkhout, 2006):

$$D = D_0 + AD \quad (14)$$

and define monitor surveys as:

$$D' = D'_0 + D'_0A'D'. \quad (15)$$

Due to change in acquisition system and surface conditions  $A$  and  $A'$  can be different for real data sets, however, dealing with synthetics allows to keep them constant. To account for reservoir parameters equation (15) can be further divided into smaller variables (Berkhout and Verschuur, 2005):

$$D_{diff} = (D_0 + D_0A'D') + (\delta D_0 + \delta D_0A'D'), \quad (16)$$

where  $\delta D_0$  denotes reservoir and overburden responses due to production. Note equation (16) is the non-conventional differencing, that is base study,  $D_0$ , monitor study,  $\delta D_0$ , and surface conditions, when surveying base and monitor study,  $D_0A'D'$ ,  $\delta D_0A'D'$ , respectively.

The use of inverse data space is hence summarized in five steps:

I. Conversion of data from FDS to IDS through least-squares algorithm, that is  $D_0 \Rightarrow D'_0$ .

II. Separation of surface operators from reflection data in Radon domain; that is further ignored for synthetic data.

III. Conversion of reflection data from IDS to FSD, that is  $D'_0 \Rightarrow D_0$ .

IV. Identify surface transfer function, in FDS and IDS, that is  $X_0 = -AD_0$  and  $X'_0 = -A'D'_0$ .

V. Compute difference data employing least-squares subtraction to obtain  $\delta X_0 = X_0 - F_{ls}X'_0$ , where  $F_{ls}$  is a scaled version of the correlation between the overburden Green's functions of the base and monitor data set (Berkhout and Verschuur, 2005). The improved difference modelling is expected to capture large and small scale physical changes as well as some amplitude patterns.

## EXAMPLES

### Velocity Models

The saturation models, through Gassmann relations, deliver velocity models in time-lapse (Milicevic and Ferguson, 2009).

The velocity models are mirrored over the left hand side and padded on bottom and top to accommodate for energy to propagate and avoid wraparound (Ferguson, personal communication). We pad a linear velocity matrix from about  $0m$  to about  $1450m$  of depth and a constant velocity matrix from about  $1950m$  to about  $3900m$  of depth. Now, the velocity trend resembles linear, square root and a constant function. Figure 1 shows the end result of the modified velocity models after day 1, 14 and 28. The two injectors are situated in the lower left and right corners and the producer at their half distance. Note the velocity and water saturation increase with time.

### Zero-offset Synthetic Seismogram Models

The velocity models are passed to a finite-difference function MATLAB CREWES Project toolbox holds, *afd\_explode*, that simulates exploding reflector concept. 2D synthetic seismograms are produced.

Figure 2 shows zero-offset synthetics created after day 1, 14 and 28. The reservoir top and bottom are denoted by arrows 4 and 1, respectively. Note reservoir top and bottom as stationary events in time-lapse at about  $1.6s$  and  $2.1s$ , respectively. The reservoir top and bottom show as a horizontal and hyperbolic events, respectively. The two waterfronts are denoted by arrows 2 and 3 on synthetic models and create a bow-tie effect. Note two water-fronts as nonstationary reflections, as they advance in time from about  $1.95s$  to about  $1.6s$ . The reservoir top amplitude is dark gray. The reservoir bottom amplitude is almost white followed by dark gray-to-black reflection. These two reflections of different polarity are due to high velocity contrast between oil and water saturated zones. The waterfronts are of almost black, white and black amplitude sequence. The overall amplitude of the reservoir dims with water saturation increase. Note horizontal linear trends to reflect injected water.

## Migrated Models

Previously generated 2D zero-offset synthetics in time,  $t$ , and distance,  $d$ , domain are converted to frequency,  $f$ , and wavenumber,  $k_x$  domain invoking Fast Fourier Transform (FFT) and Inverse Fast Fourier Transform (IFFT) (Ferguson and Margrave, 2005). The  $f$  axis is band-limited and positive and the  $k_x$  axis is not centered. Then, data is migrated calling *ss\_zero\_mig*, a MATLAB routine of the CREWES Project toolbox. The routine performs SSF depth migration (Ferguson, 2009b).

Figure 3 illustrates migrated sections after day 1, 14 and 28. The expected events, such as reservoir top and bottom, denoted by arrows 4 and 1, respectively, appear stationary. The amplitudes correspond to the amplitudes of the zero-offset unmigrated sections. The reservoir top and bottom are captured at about depth of 1450m and 1950m, respectively. The reservoir top again shows as a horizontal event, still gray, but better focused. The reservoir bottom instead of a hyperbola shows as horizontal and also better focused. Its amplitude is purely black followed by a purely white color. The waterfronets, denoted by arrows 2 and 3, propagate upwards with time. The reservoir overall amplitude still shows linear reflections where saturated with water. These reflections are better focused and more white.

## Conventionally Differenced Models

We conventionally difference migrated sections. Figure 4 (a) is a plot of conventional difference between day 1 and 14. The reservoir top is not identifiable, as it is of the same amplitude on both models. The amplitude of reservoir bottom is of reverse polarity when compared to migrated sections, namely black and white. The reservoir bottom, denoted by arrow 1, is not a horizontal event, but an intersection of curves described as square root function and its inverse. The waterfronets, denoted by arrows 2 and 3, are of the same amplitude as they are on migrated section of day 1 and 14, at depths of 1750m and 1625m, respectively. The amplitude of oil is purely white. The amplitude of the reservoir zone saturated by water is black, where as it is white to light gray on both migrated models.

Figure 4 (b) is a plot of conventional difference between days 1 and 28. Similarly, reservoir top cannot be observed on differenced models. Reservoir bottom follows the same pattern as in Figure 4(a). The reservoir bottom is almost entirely horizontal event, it is an intersection of two almost straight lines. The waterfronets are of the same amplitude as they are on migrated section of day 1 and 28, at depths of 1750m and 1450m, respectively. The amplitude of the reservoir zone saturated by water is purely white, where as it is white to light gray on both migrated models before differencing.

## Non-conventionally Differenced Models

We difference the same set of migrated sections employing the non-conventional differencing method based on Berkhouit and Verschuur (2005). Figure 4 (c) is a plot of non-conventional difference between days 1 and 14. Reservoir top cannot be observed where as reservoir bottom is a white linear reflection. It is clear to note the waterfronets, denoted by arrows 2 and 3, belong to their progression after day 1 and 14. The area between water-

fronts is defined by weak white amplitude. It has been oil saturated and replaced by water as waterfronts progress after day 1 to day 14. The area below waterfront 2 shows even more weak white amplitude, associated with primarily water saturation. The remaining oil reserves are hard to identify as weak white amplitude.

Figure 4(d) is a plot of non-conventional difference between days 1 and 28. Reservoir bottom again shows as a strong white linear amplitude and reservoir top cannot be identified. Waterfronts, denoted by arrows 2 and 3, image their progression after day 1 and 28. The area between waterfronts is defined by weak white amplitude and it is the area of oil produced between day 1 and 28. Water saturation prior to day 14 shows as weak white amplitude.

Conventional differencing proves to be of limited use in reservoir characterization as it captures no certain amplitude patterns. Non-conventional differencing proves to be an improved tool in reservoir characterization although identification areas of remaining oil seems hard. Hence, method triggers future improvement.

## CONCLUSION

Conventional seismic difference analysis study is performed on a 100 % oil saturated reservoir in time-lapse. 2D variable velocity matrix is created. Velocity matrix, invoking finite-difference algorithm and simulating exploding reflector concept, generates zero-offset synthetic seismograms in time-lapse. Synthetics are migrated using Split-step Fourier algorithm. Migrated sections are conventionally and non-conventionally differenced and compared. Conventional seismic differencing presents little value to reservoir characterization and optimization as it does not capture certain amplitude patterns. Non-conventional seismic differencing presents some improvement to reservoir characterization, however, triggers advancements as remaining oil in reservoir is hard to interpret. Linear algebra and pre-stack depth migration imaging are anticipated tools for differencing improvements.

## FUTURE WORK

We show the non-conventional seismic differencing improves imaging for use in time-lapse studies as it captures some amplitude patterns. We plan to implement improvements to the existing code using pre-stack depth migration algorithm and inverse data space to make its results more significant to remaining reserves imaging. Also, the algorithm is to be adapted for application in 3D time-lapse studies.

## ACKNOWLEDGMENT

We thank CREWES Project directors, staff, students and sponsors for support of this research.

## FIGURES

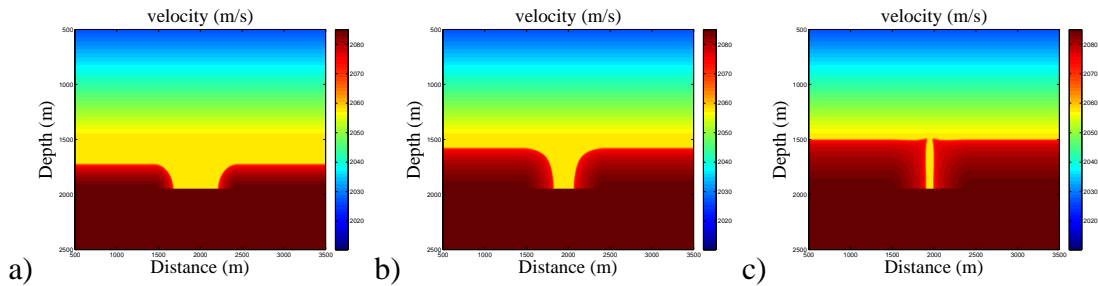


FIG. 1. Padded velocity models describing 100 % oil saturated sandstone reservoir. Models (a), (b) and (c) show reservoir as water saturation increases. Two injectors are situated in lower left and right corners, while producer sits at half distance between them. P-wave velocity decreases from injector to producer in time-lapse steps after day  $\tau = 1, 14, 28$ , respectively.

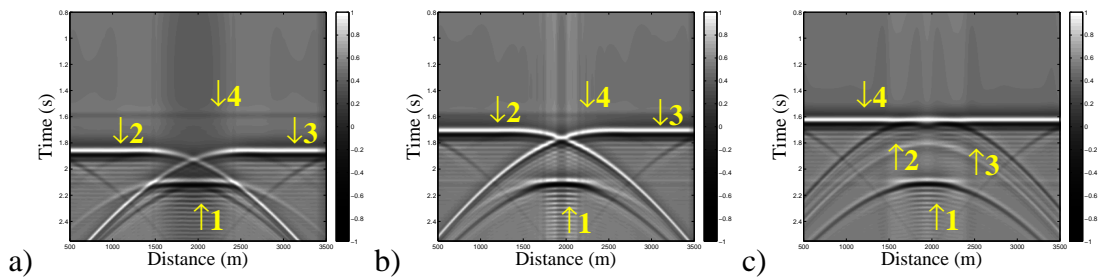


FIG. 2. 2D synthetic seismic models generated employing exploding reflector algorithm. Models (a), (b) and (c) show reservoir in time-lapse steps after day  $\tau = 1, 14, 28$ , respectively. Reservoir bottom and top, denoted by arrows 1 and 4, respectively, stay stationary in time. Arrows 2 and 3 mark waterfronts as they progress upward in time. Oil amplitude is gray. Water saturated zones show linear trends.

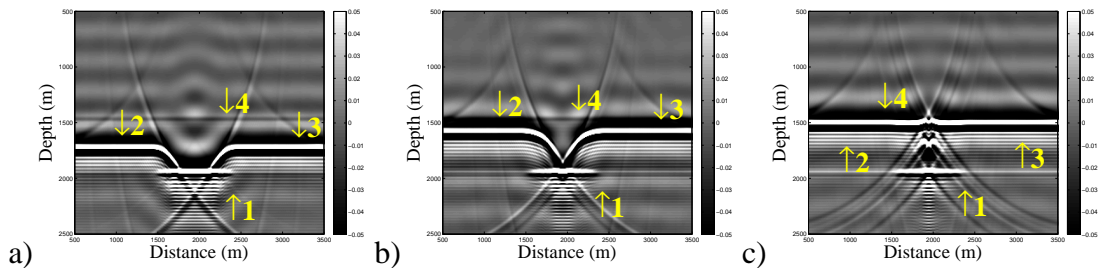


FIG. 3. Split-step Fourier migrated seismic sections generated from velocity and synthetic models. Sections (a), (b), (c) capture flattening of hyperbolic events after day  $\tau = 1, 14$  and  $28$ , respectively. Arrows 1 and 4 point to the stationary events reservoir bottom and top, respectively. Arrows 2 and 3 point to two waterfronts propagating upwards in time. Oil amplitude is light gray and better focused. Water saturated zones capture linear trends and as well are better focused.

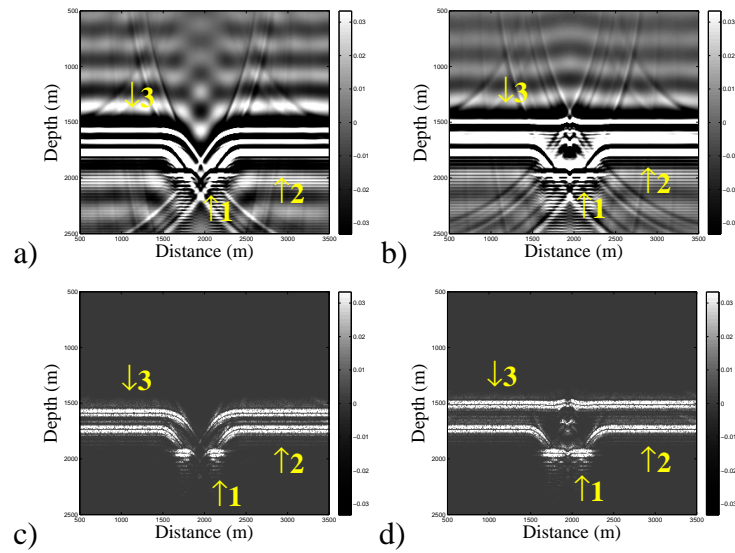


FIG. 4. Differenced migrated models. Models (a) and (b) capture conventional difference of models after days 1 and 14 and days 1 and 28, respectively. Models (c) and (d) capture non-conventional difference of models after days 1 and 14 and days 1 and 28, respectively. Arrow 1 denotes reservoir bottom, whereas, no reservoir top reflection can be identified. Arrows 2 and 3 mark two waterfronts corresponding to differenced models. Produced areas are easily identifiable on non-conventionally differenced models. It is hard to identify areas of remaining production on both conventional and non-conventional differenced models.

## REFERENCES

- Aarnes, J. E., T. Gimse, and K. A. Lie, 2007, An introduction to the numerics of flow in porous media using MATLAB, *in* Numerical Simulation, and Optimization: Applied Mathematics at SINTEF: Springer, 265–306.
- Berkhout, A. J., 2006, Seismic processing in the inverse data space: *Geophysics*, **71**, 29–33.
- Berkhout, A. J., and D. J. Verschuur, 2005, Time lapse processing in the inverse data space: 75th Ann. Internat. Mtg., Soc. Expl. Geophys., Expanded Abstracts, 1522–1525.
- Bertrand, A., S. McQuaid, R. Bobokecki, and S. Leiknes, 2005, A high resolution workflow for 4d-friendly analysis: Application to gas-oil contact monitoring at troll west: 75th Ann. Internat. Mtg., Soc. Expl. Geophys., Expanded Abstracts, 2422–2425.
- Cheng, A., L. Huang, and J. Rutledge, 2009, Time-lapse VSP data processing for monitoring CO<sub>2</sub> injection: 79th Ann. Internat. Mtg., Soc. Expl. Geophys., Expanded Abstracts, 406–410.
- Christie, M. A., and M. J. Blunt, 2001, Tenth SPE comparative solution project: A comparison of upscaling techniques: SPE Reservoir Engineering and Evaluation, Society of Petroleum Engineers, **4**, 308–317.
- Cosse, R., 1993, Basics of reservoir engineering: Oil and Gas Field Development Techniques: Editions TECHNIP.
- Du, Y., 2007, Prestack depth migration methods for isotropic and polar anisotropic media: PhD thesis, University of Calgary.
- Ferguson, R. J., 2009a, Theory of seismic imaging: Course notes, University of Calgary.
- Ferguson, R. J., 2009b, Crewes 2D depth migration in matlab: A new release: CREWES Research Report, **21**, 1–9.
- Ferguson, R. J., and G. F. Margrave, 2005, Planned seismic imaging using explicit one-way operators: *Geophysics*, **70**, 101–109.
- Ferguson, R. J., and G. F. Margrave, 1999, A practical implementation of depth migration by nonstationary phase shift: 69th Ann. Internat. Mtg., Soc. Expl. Geophys., Expanded Abstracts, 1370–1374.
- Huang, X., L. Meister, and R. Workman, 1998, Improving production history matching using time-lapse seismic data: *The Leading Edge*, **17**, 1430–1433.
- Inannen, K., 2010, Signal analysis: Course notes, University of Calgary.
- Inannen, K., 2009, Inverting absorptive reflections: an inverse series tutorial: CREWES Research Report, **21**, 1–13.
- Jin, L., and X. Chen, 2008, The combination of wavelet transform and nonlinear filtering for time-lapse seismic difference analysis: 78th Ann. Internat. Mtg., Soc. Expl. Geophys., Expanded Abstracts, 3214–3218.
- Lines, L. R., and R. Newrick, 2008, Geophysical interpretation: SEG.
- Mi, Y., 2002, Prestack depth imaging and velocity analysis for p-p and p-s data with nonstationary integral extrapolators: PhD thesis, University of Calgary.
- Milicevic, V., and R. J. Ferguson, 2009, Numerical fluid flow modelling and its seismic response in time-lapse: CREWES Research Report, **21**, 1–13.
- Schinelli, M., 2006, Using complex seismic attributes to improve 4d visibility of fluid contact movement: 66th Ann. Internat. Mtg., Soc. Expl. Geophys., Expanded Abstracts, 3295–3298.
- Stoffa, P. L., J. T. Fokkema, R. M. de Luna Freire, and W. P. Kessinger, 1990, Split-step

- Fourier migration: *Geophysics*, **55**, 410–421.
- Vracar, B., 2007, Pressure transient analysis: Technical report, SAIT.
- Zou, Y., L. R. Bently, and L. R. Lines, 2004, Integration of geophysical methods with reservoir simulation: 74th Ann. Internat. Mtg., Soc. Expl. Geophys., Expanded Abstracts, 1623–1626.